energy&fuels

Article

pubs.acs.org/EF

Asphaltene Deposition in Different Depositing Environments: Part 2. Real Oil†

Mohammad Tavakkoli,[‡,§] Sai R. Panuganti,[‡] Vahid Taghikhani,[§] Mahmoud Reza Pishvaie,[§] and Walter G. Chapman*[,‡]

[‡]Department of Chemical and Biomolecular Engineering, Rice University, Houston, Texas 77005, United States

[§]Department of Chemical and Petroleum Engineering, Sharif University of Technology, Tehran, Iran

ABSTRACT: This paper is a continuation of our previous paper (part 1; 10.1021/ef401857t), which discussed the roles of different phenomena effecting the deposition of asphaltene from model oil systems and before the onset of asphaltene precipitation. The study in this paper is to understand the depositional tendency of asphaltene using a quartz crystal microbalance with dissipation (QCM-D) measurements and their corresponding modeling for real crude oil systems with emphasis after the onset of asphaltene precipitation.

1. INTRODUCTION

In our previous paper (part 1; 10.1021/ef401857t), we discussed that, to improve asphaltene deposition mitigation technologies, knowledge of the deposition mechanism of asphaltene and the factors influencing deposition is needed for many different domains of the oil industry.[1] Quartz crystal microbalance with dissipation (QCM-D) experiments are performed here to study different depositional aspects of asphaltene from model oil (part 1; 10.1021/ef401857t) and real crude oil (part 2) systems. Although a few researchers have used a quartz crystal microbalance for investigating asphaltene adsorption kinetics, they were all limited to model oil systems. To our knowledge, only Abudu and Goual used crude oil for QCM-D adsorption measurements.[2] They used crude oil in different solvents under flow conditions. In toluene, Langmuir-type adsorption was recorded with saturation film thicknesses of 3−4 nm and limited desorption after rinsing. In *n*-alkanes (*n*-heptane, *n*-decane, and *n*-pentadecane), saturation plateaus were not observed within the experimental time scale. Film thicknesses recorded after 3.5 h were all higher than those in toluene and increased with an increasing *n*-alkane carbon number.

In our previous paper (part 1; 10.1021/ef401857t), a model is presented for the first time in the literature to capture the asphaltene adsorption process in QCM-D before the precipitation onset. However, the asphaltene depositional problems in a wellbore and pipeline are also associated with asphaltene precipitation issues. An insufficient understanding of asphaltene deposition mechanisms after precipitation onset lead to only a few modeling studies being published in the literature. Ramirez et al. described the usage of a molecular diffusion model to represent asphaltene deposition, assuming that the particle concentration gradient is caused by the temperature gradient at the wall.[3] However, the asphaltene deposition rate is not affected by the temperature gradient.[4] Jamialahmadi et al. developed an experimental setup to measure the thickness of the asphaltene deposit based on change in resistivity of the boundary layer.[5] Their mechanistic model for asphaltene deposition failed to take into account the aggregation process. Zhu et al. performed three-phase computational fluid dynamic calculations for determining the asphaltene deposition and concluded that the deposition in bend and sudden changed pipelines is greater than that in straight pipelines.[6]

Sileri et al. focused on modeling of asphaltene deposition in a crude preheat train.[7] This is the only work that incorporated aging phenomena of asphaltene (even though empirical). Nevertheless, their focus was on displacement and removal of an initial uniformly distributed layer of deposit at the walls. Recently, Eskin et al. used particle flux mass-transfer expressions for turbulent flows to model the deposition process.[8] The required model parameters are obtained by fitting the model predictions to the deposition results obtained from their coquette flow device. Vargas et al. proposed a deposition simulator based on species conservation coupled with thermodynamic modeling of oil with the perturbed chain statistical associating fluid theory (PC-SAFT).[9] A capillary scale setup was used to estimate the parameters required in the model. The work by Vargas et al. was extended and developed into a field-scale computationally efficient deposition simulator called the asphaltene deposition tool (ADEPT) by Kurup et al., who discussed asphaltene deposition in a few field cases.[10,11]

This paper investigates crude oil asphaltene−surface interactions through characterization of the deposition behavior on various surfaces using QCM-D under flow conditions. The main surface type used for experiments involving crude oil is carbon steel. Different mathematical models are used to model the experimental data obtained in this study for before and after the asphaltene precipitation onset, because of the different deposition mechanisms before and after precipitation. The effect of the surface type on the deposition after precipitation is discussed on the basis of carbon steel, iron oxide, and gold sensors. Throughout the paper, the "part 1" paper refers to our

†Presented at the 14th International Conference on Petroleum Phase Behavior and Fouling.

Received: September 17, 2013
Revised: April 14, 2014
Published: April 15, 2014

previous paper (10.1021/ef401857t),[1] and the "part 2" paper refers to the current paper.

2. EXPERIMENTAL SECTION

For this paper, experiments are conducted to investigate the deposition behavior of asphaltene on metal surfaces from crude oil. The same crude oil (S) used for extracting asphaltene to prepare model oil solutions in the "part 1" paper (10.1021/ef401857t) is used here directly. Table 1 shows the properties of crude oil (S). The experimental procedures for asphaltene adsorption experiments using QCM-D and determination of asphaltene precipitation onset have already been described in our previous paper (part 1; 10.1021/ef401857t). The same equipment, parts, and setup from the model oil study (part 1; 10.1021/ef401857t) are retained for the QCM-D study with crude oils.

Table 1. Crude Oil (S) Properties at 1 atm and 20 °C

property	value
density (g/cm^3)	0.843
molecular weight (g/mol)	193
viscosity (cP)	9.5
saturate (wt %)	66.26
aromatic (wt %)	25.59
resin (wt %)	5.35
n-C_5 asphaltene (wt %)	2.80

In this study, using crude oil directly eliminates the need for asphaltene extraction. All of the reagents used here are high-performance liquid chromatography (HPLC)-grade and procured from Sigma-Aldrich. All experimental solutions are freshly prepared before the start of the experiment. Before the solutions were prepared, crude oil is filtered using a 0.2 μm nylon filter paper to remove undesirable large particles, which can plug the flow system.

Unlike model oils, where solvents of known properties are used, the density and viscosity of crude oil solutions had to be measured for deposition modeling purposes. Dynamic viscosity is calculated from kinematic viscosity measurements using a calibrated Cannon-Fenske viscometer of size 50. The method involves measuring the flow time of Newtonian liquids in a capillary with an accuracy of 1 s. A glass pycnometer with 5 mL capacity is used to measure the liquid density.

3. MODELING

3.1. Frequency and Dissipation Changes. In QCM-D experiments, interpreting the frequency and dissipation changes (Δf and ΔD, respectively) in terms of mass/thickness and properties of the deposit have already been discussed in our previous paper (part 1; 10.1021/ef401857t).[1] Figure 1 presents frequency and dissipation changes versus time for the adsorption of asphaltene from a crude oil + n-heptane + toluene system (10:70:20) onto a carbon steel crystal surface. Δf and ΔD in Figure 1 represent an adsorbed viscoelastic film because of the following observations: (1) spreading of the overtones in Δf and ΔD responses and (2) $|\Delta D/\Delta f|$ being comparable to 0.4×10^{-6} Hz^{-1}.[12]

In this study, all experiments for crude oil plus heptol (mixture of n-heptane and toluene) showed viscoelastic behavior for the deposited asphaltene layer onto a crystal surface. Hence, the Voigt model, available in the QTools software from Q-Sense, is used for viscoelastic interpretation of frequency and dissipation changes. The resultant deposited mass is treated as experimental data like all other QCM-D experiments in the literature.

3.2. Adsorbed Mass Modeling before Onset. In this paper, the term "deposition" is used in general for any process of asphaltene adhesion onto a solid surface. Before asphaltene precipitation onset, where all asphaltenes are stable in the system, the term "adsorption" may also be used. After precipitation onset, only the term "deposition" is used throughout the paper.

In our previous paper (part 1; 10.1021/ef401857t), a kinetic–diffusive–convective model is presented and used for QCM-D asphaltene adsorption modeling (from model oil) before the precipitation onset. The same model is applied here for asphaltene adsorption from crude oil solutions. The model is based in part on the equations proposed by Filippov.[13]

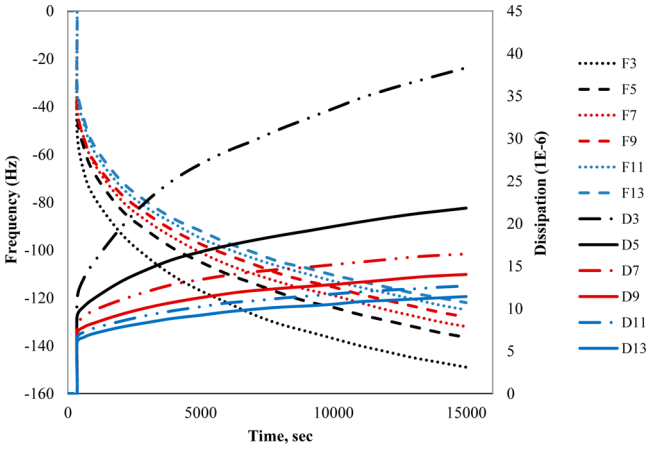

Figure 1. Frequency and dissipation changes versus time for the adsorption of asphaltene from a crude oil + n-heptane + toluene system (10:70:20) onto a carbon steel crystal surface at 20 °C.

3.3. Deposited Mass Modeling after Onset. The mechanism of adsorption before and after the asphaltene precipitation onset is different, because of the effects of precipitation and aggregation of the precipitated asphaltene coming into picture after the onset. Hence, the model proposed in our previous paper (part 1; 10.1021/ef401857t) for asphaltene adsorption before the onset cannot be used after the precipitation has occurred. For this study, the mechanism proposed by Vargas et al. for asphaltene deposition in capillary-scale experiments is used here for QCM-D experiments.[9]

After asphaltene precipitation, the transport of asphaltene over the crystal in the flow module may follow a multi-step process, including precipitation, aggregation, advection, diffusion, and deposition. The mechanism is summarized pictorially in Figure 2. According to the mechanism, asphaltene precipitation leads to the appearance of primary particles, represented in Figure 2 as small dark circles. These particles can stick to one another undergoing an aggregation process, forming bigger particles, or can follow a diffusion mechanism to the surface of the crystal, where they can adhere to the surface and build up a deposit. Additionally, all particles are transported in the flow direction by the advection process. The flow is in laminar regime, and the Peclet number is very high for all of the QCM-D experiments studied here.

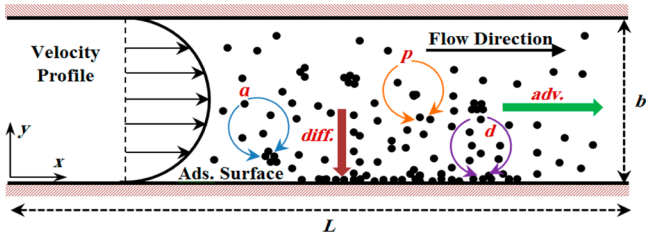

Figure 2. Mechanism of asphaltene deposition in a QCM-D flow module: *adv.*, advection; *diff.*, diffusion; *a*, aggregation; *p*, precipitation; and *d*, deposition.

All of these phenomena can be incorporated into a mathematical model that tracks the transport of primary asphaltene particles. The material balance in the transient state for these primary particles is represented by eq 1, where the rates are considered as first order

$$\frac{\partial c}{\partial t} = -V_x(y)\frac{\partial c}{\partial x} + D\frac{\partial^2 c}{\partial y^2} + k_p(c_0 - c^{eq})\exp\left(-k_p\frac{x}{\langle V_x(y)\rangle}\right) - k_{ag}c \quad (1)$$

subject to the following boundary and initial conditions:

$$\frac{\partial c}{\partial y} = 0 \text{ at } y = \frac{b}{2}, \text{ for all } x \tag{2}$$

$$c = c_i \text{ at } x = 0, \text{ for all } y \tag{3}$$

$$D\frac{\partial c}{\partial y} = k_d c \text{ at } y = 0, \text{ for all } x \tag{4}$$

$$c = c_i \text{ at } t = 0, \text{ for all } x \text{ and } y \tag{5}$$

where c is the concentration of the asphaltene primary particle in the flow cell, x is the coordinate in the direction of flow, y is the coordinate in the direction normal to the flow, t is the time, $V_x(y)$ is the axial linear velocity, $\langle V_x(y)\rangle$ is the average axial velocity, D is the diffusion coefficient, c_0 is the concentration of asphaltene in solution at inlet conditions, c^{eq} is the concentration of dissolved asphaltene at equilibrium, k_p is the precipitation rate constant, k_{ag} is the aggregation rate constant, k_d is the deposition rate constant, and c_i is the concentration of primary particles at initial conditions.

In eq 1, the rate of asphaltene precipitation, r_p, is assumed to be proportional to the supersaturation degree of asphaltene, which is defined as the difference between the actual concentration of asphaltene dissolved in the oil and the concentration of asphaltene at equilibrium, according to eq 6.

$$r_p = k_p(c_0 - c^{eq})\exp\left(-k_p\frac{x}{\langle V_x(y)\rangle}\right) \tag{6}$$

The rates of asphaltene aggregation and deposition, r_{ag} and r_d, are defined by eqs 7 and 8, respectively.

$$r_{ag} = -k_{ag}c \tag{7}$$

$$r_d = -k_d c \tag{8}$$

The details of the mathematical model can be found in the work by Vargas et al.[9]

The proposed model is implemented in the transient form to capture the experimental data against time obtained using the QCM-D experiments. A conventional numerical technique of finite differences is used for solving the partial differential eq 1 with the corresponding conditions. The PC-SAFT equation of state is applied for calculating the concentration of dissolved asphaltene at equilibrium. The procedure for obtaining the PC-SAFT parameters for oil fractions and asphaltene is well-established in the literature.[14−16] Also, the PC-SAFT parameters for the crude oil (S) used in this study, are already available from the work by Panuganti et al. (crude oil A in their paper).[17]

4. RESULTS AND DISCUSSION

In this paper, a solution of crude oil in heptol (10 vol % crude oil in 90 vol % heptol) is used as the injection fluid into the QCM-D setup. A constant value for the ratio of crude oil/heptol is applied because the effect of different ratios has already been investigated by another group.[2] The ratio of 10:90 for crude oil/heptol is selected because the system of 10 vol % crude oil + 90 vol % n-heptane is well into the region of asphaltene precipitation for the crude oil + heptol system and one can easily investigate the effect of precipitating agent addition (n-heptane) beyond the precipitation onset. Later in this section, we will show that the onset of asphaltene precipitation happens near 10 vol % crude oil + 70 vol % n-heptane + 20 vol % toluene. The total asphaltene concentration is maintained constant in all of the solutions of 10 vol % crude oil + 90 vol % heptol. All experiments are performed at 20 °C and 80 μL/min flow rate. As shown in the Modeling section, all experimental results showed a viscoelastic behavior of the deposited layer from the crude oil + heptol system. Therefore, the Voigt model in the QTools software is applied for deposited mass interpretation from frequency and dissipation changes of the sensor crystal.

In this study and in our previous paper (part 1; 10.1021/ef401857t), each experiment is performed 3 times and the average deposited mass is reported. As observed from Figure 1, all of the experimental data are smooth. Also, the results obtained from Voigt modeling show continuous smooth curves for the amount of deposited mass versus time. Error bars are plotted in Figure 3 on some of the data points to show that the experiments

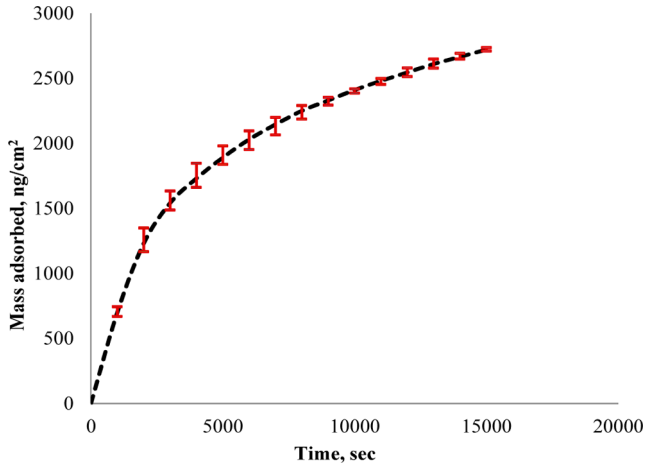

Figure 3. Adsorbed mass amount from the n-C_5 asphaltene + toluene system onto a gold crystal surface versus time at 80 μL/min flow rate and 60 °C with the error bars.

are reasonably repeatable. In Figure 3, there are over 15 000 data points to plot error bars on all of the data points. The average standard deviation of the data points with error bars is 2.33%.

4.1. Elimination of the Liquid Loading Effect. Unlike the model oil system (asphaltene in heptol), the viscosity and density variations caused by the introduction of crude oil into heptol imply that liquid loading effects have a non-negligible role in the QCM-D response.[18] Using eqs 9 and 10, changes in both frequency and dissipation because of liquid loading effect can be calculated[18]

$$\Delta f_{\text{liquid loading}} = -\sqrt{\frac{n}{\pi}}\frac{f_0^{3/2}}{\rho_q \nu_q}\left(\sqrt{\rho_l \eta_l} - \sqrt{\rho_s \eta_s}\right) \tag{9}$$

$$\Delta D_{\text{liquid loading}} = -\frac{1}{\sqrt{n\pi}}\frac{2f_0^{1/2}}{\rho_q \nu_q}\left(\sqrt{\rho_l \eta_l} - \sqrt{\rho_s \eta_s}\right) \tag{10}$$

where f_0 is the fundamental resonant frequency ($f_0 = 5 \times 10^6$ Hz), n is the overtone number ($n = f_n/f_0 = 1, 3, 5, 7, 9, 11$, and 13), ρ_q is the specific density of quartz (2650 kg/m^3), ν_q is the shear wave velocity in quartz (3340 m/s), $\nu_q = (\mu_q/\rho_q)^{1/2} = 2f_0 h_q$, μ_q is the shear modulus of quartz (2.947×10^{10} Pa), h_q is the thickness of the quartz crystal (3.37×10^{-4} m), ρ is the density, η is the viscosity, and subscripts s and l refer to the solvent and liquid mixtures, respectively.

Table 2 shows the calculated $\Delta f_{\text{liquid loading}}$ and $\Delta D_{\text{liquid loading}}$ for the third harmonic overtone of the 10 vol % crude oil + 90 vol % heptol system at different ratios of n-heptane/toluene. Similar calculations are performed for all other overtones, and after eliminating the effect of liquid loading from the total Δf and ΔD, one can find the net change in frequency and dissipation with time, which are due to the deposited solid particles onto the

dx.doi.org/10.1021/ef401868d | Energy Fuels 2014, 28, 3594−3603

Table 2. Calculated $\Delta f_{\text{liquid loading}}$ and $\Delta D_{\text{liquid loading}}$ for the Third Harmonic Overtone and at Different Ratios of *n*-Heptane/Toluene

oil/heptane/toluene ratio	liquid density (g/cm^3)	liquid viscosity (cP)	$\Delta f_{\text{liquid loading}}$ (Hz)	$\Delta D_{\text{liquid loading}}$ ($\times 10^{-6}$)
10:0:90	0.864	0.721	−30.59	12.24
10:20:70	0.828	0.645	−28.65	11.46
10:40:50	0.791	0.586	−26.24	10.50
10:60:30	0.755	0.571	−30.33	12.13
10:70:20	0.736	0.545	−28.88	11.55
10:80:10	0.718	0.536	−29.67	11.87
10:90:0	0.700	0.531	−39.42	15.77

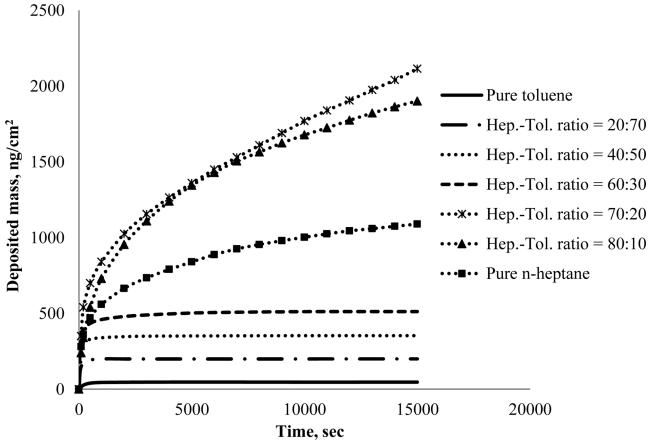

Figure 4. Deposited mass versus time from solutions of 10 vol % crude oil + 90 vol % heptol onto the surface of carbon steel sensor crystal at different ratios of *n*-heptane/toluene at 20 °C and 80 μL/min flow rate after eliminating the liquid loading effects.

surface of the sensor crystal. Thus, Figure 4 is the resultant amount of deposited mass versus time for different ratios of *n*-heptane/toluene after eliminating the liquid loading effect. The liquid trapping effect is negligible because of the use of a smooth sensor crystal surface.

4.2. Modeling of the Model Oil System after Onset. Our previous paper (part 1; 10.1021/ef401857t) was limited to modeling of the adsorption process in QCM-D before the precipitation of asphaltene. In this paper, with the introduction of deposition modeling in QCM-D after the precipitation of asphaltene, the model oil system is explored first before applying for real crude oil systems. As presented in our previous paper (part 1; 10.1021/ef401857t), a 100 ppm asphaltene in heptol solution resulted in Figure 5 for deposited mass with time. Asphaltene precipitation onset for the model oil system happens near 55 vol % *n*-heptane based on the results obtained in our previous paper (part 1; 10.1021/ef401857t). From Figure 5, the maximum amount of asphaltene deposition occurs near the asphaltene precipitation onset for the model oil system. After precipitation onset, asphaltenes aggregate, forming larger particles, which can pass over the sensor crystal surface without depositing because of convective transfer.

To calculate the concentration of dissolved asphaltene at equilibrium, c^{eq}, the PC-SAFT equation of state is applied. The PC-SAFT has previously shown modeling results matching experimental observations for the onset of precipitation and the precipitated amount from solvent-diluted crude oils at different concentrations of precipitating agents.[19] This is possible because

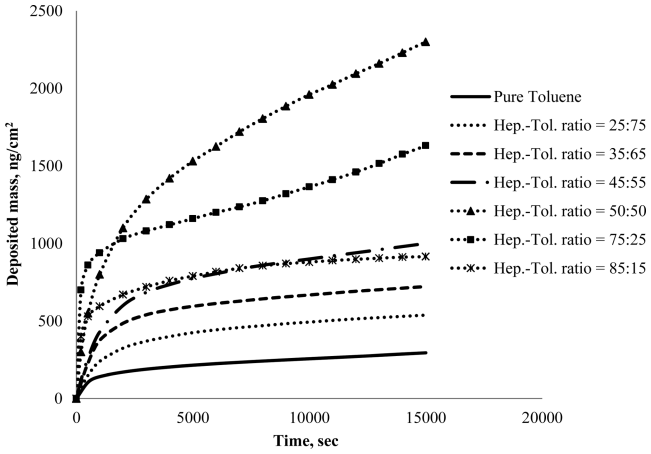

Figure 5. Deposited mass from the *n*-C_7 asphaltene + heptol systems onto a gold crystal surface versus time at 20 °C and 80 μL/min flow rate.

of the correct estimation of the concentration of dissolved asphaltene at equilibrium, c^{eq}. Therefore, the PC-SAFT can rightly calculate the values of c^{eq} at various concentrations of *n*-heptane in both the model oil and real oil systems. The calculated c^{eq} in the case of 75:25 for the *n*-heptane/toluene ratio is 0.07482 g/m^3, and the calculated c^{eq} in the case of 85:15 for the *n*-heptane/toluene ratio is 0.001 863 g/m^3.

The diffusion coefficient (D) and kinetic constants of precipitation (k_p), aggregation (k_{ag}), and deposition (k_d) are the four adjustable parameters tuned to reproduce the experimental data for the amount of deposited mass beyond the onset of asphaltene precipitation, i.e., for 75 and 85 vol % *n*-heptane. These adjusted values are presented in Table 3. Figures 6 and 7 show the

Table 3. Adjusted Values of the Parameters Used To Reproduce the Experimental Data for the Amount of Deposited Mass beyond the Onset of Asphaltene Precipitation in a 100 ppm Asphaltene Model Oil Solution at 20 °C

parameter	75 vol % *n*-heptane	85 vol % *n*-heptane
D (m^2/s)	9.00×10^{-10}	1.00×10^{-10}
k_p (s^{-1})	2.90×10^{-3}	2.90×10^{-3}
k_{ag} (s^{-1})	5.20×10^{-5}	5.20×10^{-5}
k_d (m/s)	1.40×10^{-6}	1.40×10^{-6}

modeling results for the amount of deposited mass beyond the onset of asphaltene precipitation.

The operating conditions, oil, asphaltene, and depositing surface, are the same for both of the cases of 75 and 85 vol % *n*-heptane in Table 3. Hence, the kinetic constants (k_p, k_{ag}, and k_d) remain the same for both of them in Table 3. At constant conditions with a varying oil/precipitant ratio, Kurup et al. also reported the same kinetic constant values for the different oil/precipitant ratios.[11] In Table 3, the diffusion coefficient is higher for the case of 75 vol % *n*-heptane. The slightly bigger asphaltene primary particle size with an increasing instability of asphaltene in solution (higher volume percentage of *n*-heptane) results in a lower diffusion coefficient.[20]

As mentioned in our previous paper (part 1; 10.1021/ef401857t), we could not detect when the first layer of asphaltene forms on the surface of the sensor using the QCM equipment. Before this first layer, we have asphaltene−metal interactions, and after the first layer is formed, we have asphaltene−asphaltene

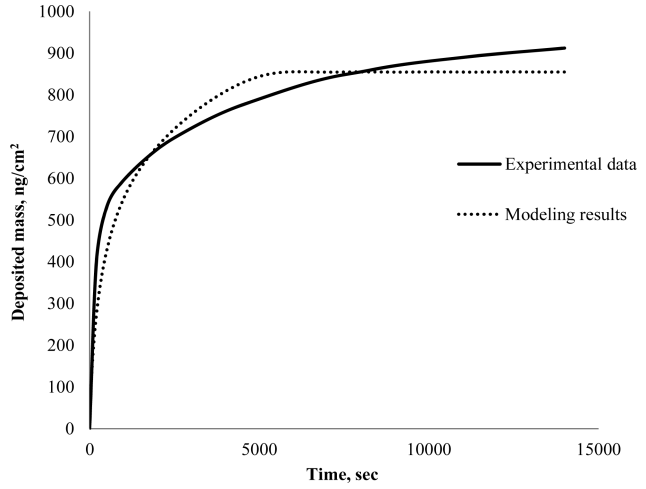

Figure 6. Experimental and modeling results of deposited mass versus time from a solution of 100 ppm n-C_7 asphaltene in heptol with 85 vol % n-heptane onto a gold surface at 20 °C and 80 μL/min flow rate.

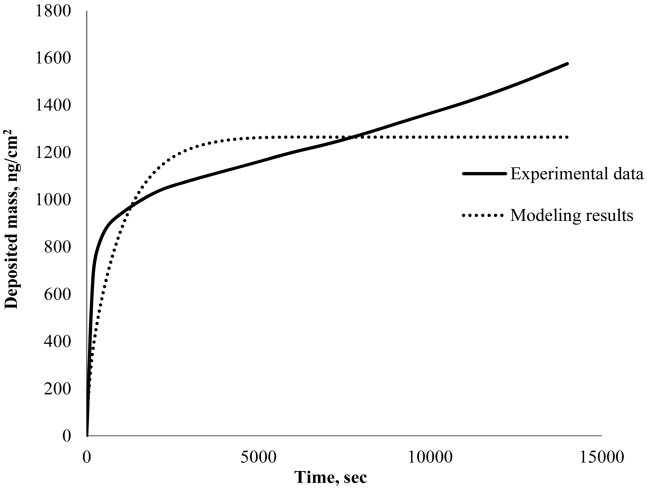

Figure 7. Experimental and modeling results of deposited mass versus time from a solution of 100 ppm n-C_7 asphaltene in heptol with 75 vol % n-heptane onto a gold surface at 20 °C and 80 μL/min flow rate.

interactions. From modeling results, one may conclude that, at the initial stage of experiments where the adsorption process is controlled by the adsorption kinetics, the asphaltene–metal interactions are dominant and, after a long time of experiments, the asphaltene–asphaltene interactions play the main role in the adsorption process.

4.3. Asphaltene Precipitation Onset of the Crude Oil + Heptol System. To find the onset of asphaltene precipitation, the method explained in our previous paper (part 1; 10.1021/ef401857t) is used. Figure 8 presents the absorbance as a function of the heptane volume percent at 500 nm ultraviolet–visible (UV–vis) wavelength. The intersection of two trend lines that pass through the data points represents the volume percent of n-heptane at the precipitation onset. For the crude oil (10%) + heptol (90%) system used in this work, the precipitation onset happens near 75.18 vol % n-heptane based on the result obtained from Figure 8.

Using different UV–vis wavelengths for measuring the absorbance gives different values of the absorbance. However, the sudden deviation in the data, which corresponds to the volume percentage of n-heptane at the precipitation onset, is

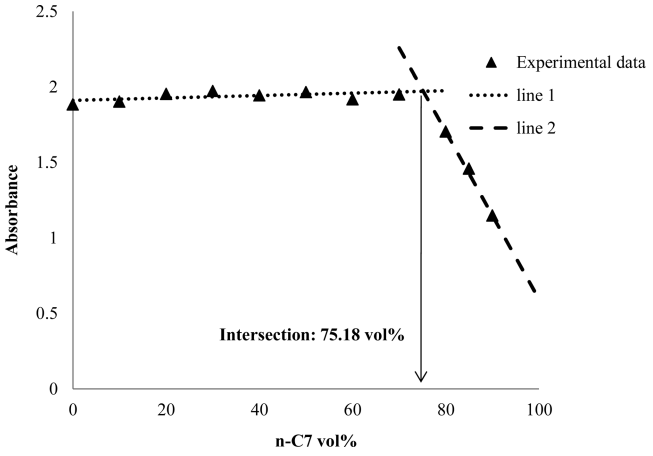

Figure 8. Precipitation onset measurement using absorbance of UV–vis at 500 nm wavelength for the crude oil (10%) + heptol (90%) system.

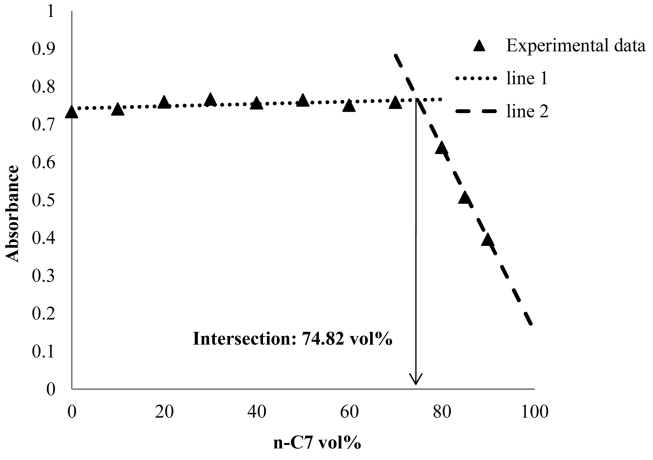

Figure 9. Precipitation onset measurement using absorbance of UV–vis at 600 nm wavelength for the crude oil (10%) + heptol (90%) system.

nearly the same. Figures 9 and 10 present the absorbance at the UV–vis wavelength of 600 and 800 nm, respectively, as a function of the n-heptane volume percentage. On the basis of the results obtained from Figures 9 and 10, the precipitation onset happens near 74.82 and 74.32 vol % n-heptane, respectively, which are very close to the value obtained at the UV–vis wavelength of 500 nm. The advantage of the procedure used here in obtaining the asphaltene precipitation onset without aggregation effects has already been discussed in our previous paper (part 1; 10.1021/ef401857t).

4.4. Modeling of the Crude Oil System before Onset. After determination of the asphaltene precipitation onset for the crude oil + heptol system, the QCM-D experimental data of the adsorbed mass before the onset are modeled using the kinetic–diffusive–convective model described in our previous paper (part 1; 10.1021/ef401857t).

In this modeling study of the experimental data before the asphaltene precipitation onset, model results showed that, for initial time, the amount of mass adsorbed is a linear function of time, which means that the rate of adsorption depends upon K_{ad} and does not depend upon parameters characterizing diffusion and convective transfer. Therefore, for this case, the adsorption process is controlled by the adsorption kinetics. The adsorption process for long times is governed by the diffusion and the convective transfer. For the experimental data in Figure 4 before

dx.doi.org/10.1021/ef401868d | Energy Fuels 2014, 28, 3594–3603

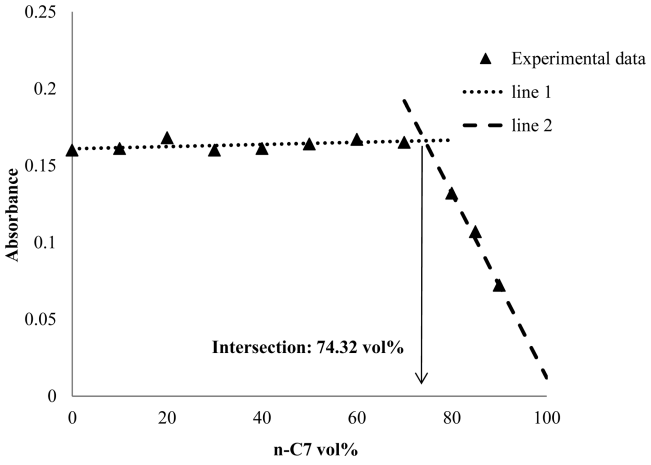

Figure 10. Precipitation onset measurement using absorbance of UV−vis at 800 nm wavelength for the crude oil (10%) + heptol (90%) system.

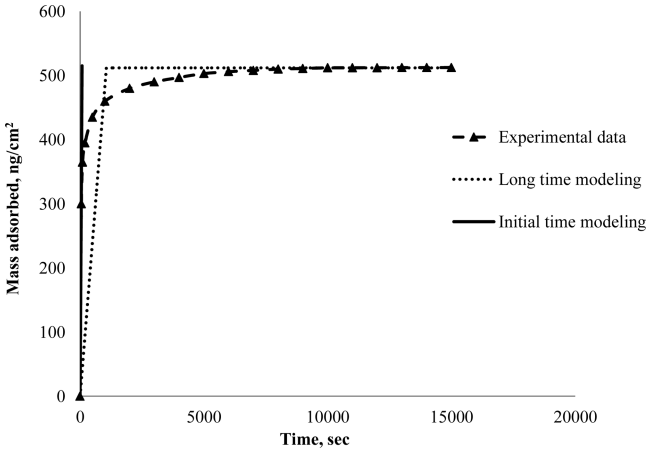

Figure 11. Experimental and modeling results for the amount of adsorbed mass from crude oil + heptol with 60 vol % *n*-heptane onto a carbon steel crystal surface versus time at 20 °C and 80 μL/min flow rate.

the onset of precipitation, all curves of deposited mass reach equilibrium very soon. Hence, a rectangular adsorption isotherm is applied to find a reasonable match. Figure 11 presents modeling results versus experimental mass adsorbed for crude oil + heptol with 60 vol % *n*-heptane.

During initial time, the values of the adsorption rate constant, which are used to model the amount of mass adsorbed from solutions of crude oil + heptol at 0, 20, 40, and 60 vol % *n*-heptane are 0.00065, 0.0011, 0.0018, and 0.0028 s^{-1}, respectively. For long times, the diffusion coefficients of 1.0×10^{-11}, 3.5×10^{-11}, 4.2×10^{-11}, and 5.0×10^{-11} are used at 0, 20, 40, and 60 vol % *n*-heptane, respectively. The experimental temperature is constant, and solution viscosity does not change much in these cases.

4.5. Modeling of the Crude Oil System after Onset. For the case of crude oil (10 vol %) + heptol (90 vol %) QCM-D experimental data reported in Figure 4, when the volume percentage of *n*-heptane increases, the amount of deposited mass increases up to 70 vol % *n*-heptane. The amount of deposited mass decreases beyond the onset volume percentage of *n*-heptane. We believe that after the asphaltene precipitation onset, the precipitated asphaltene particles aggregate, forming large particles, which can pass over the crystal surface without deposition because of convective transfer. The trend is captured by the model, as described in this section.

To calculate c^{eq}, the concentration of dissolved asphaltene at equilibrium, the PC-SAFT equation of state is applied. The obtained c^{eq} in the case of 80 vol % *n*-heptane is 53.6744 g/m^3, and the obtained c^{eq} in the case of 90 vol % *n*-heptane (pure *n*-heptane) is 1.1132 g/m^3. It should be mentioned that, in these cases, c^{eq} is very small in comparison to the c_0 value. c_0 is around 2300 ppm for C_5 asphaltenes and somewhere below 2300 ppm for C_7 asphaltenes but still much more than the c^{eq}. Therefore, here, we could model the deposition by assuming that we could substitute $c_0 - c^{eq}$ with c_0, therefore avoiding the SAFT beyond the precipitation onset. However, just to follow the proposed model for deposition and to be more precise, we have used $c_0 - c^{eq}$ in modeling the deposition process.

Table 4 presents the four adjustable parameters of the diffusion coefficient (D) and kinetic constants of precipitation (k_p),

Table 4. Adjusted Values of the Parameters Used To Reproduce the QCM-D Experimental Data of Deposited Mass beyond the Onset of Asphaltene Precipitation in Crude Oil + Heptol Solutions at 20 °C

parameter	80 vol % *n*-heptane	90 vol % *n*-heptane
D (m^2/s)	4.50×10^{-12}	1.50×10^{-12}
k_p (s^{-1})	6.40×10^{-4}	6.40×10^{-4}
k_{ag} (s^{-1})	2.10×10^{-4}	2.10×10^{-4}
k_d (m/s)	7.50×10^{-8}	7.50×10^{-8}

aggregation (k_{ag}), and deposition (k_d), which are tuned to reproduce the experimental data for the amount of deposited mass beyond the onset of asphaltene precipitation, i.e., 80 and 90 vol % *n*-heptane. Figures 12 and 13 demonstrate the modeling

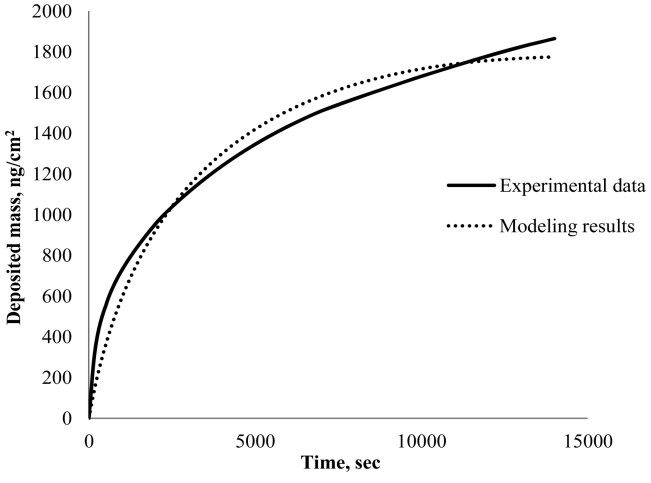

Figure 12. Experimental and modeling results of deposited mass from the 10 vol % crude oil + 90 vol % heptol solution with 80 vol % *n*-heptane onto a carbon steel surface at 20 °C and 80 μL/min flow rate.

results for the amount of deposited mass beyond the onset of asphaltene precipitation.

Similar to the explanation presented in the Modeling of the Model Oil System after Onset section, a comparison of the diffusion coefficient values reported in Table 4 shows a higher value for the case of 80 vol % *n*-heptane than that for the case of 90 vol % *n*-heptane. Also, the values of kinetic constants (k_p, k_{ag}, and k_d) are the same for both the cases of 80 and 90 vol % *n*-heptane, because operating conditions, oil, asphaltene, and depositing surface, are maintained the same.

dx.doi.org/10.1021/ef401868d | *Energy Fuels* 2014, 28, 3594−3603

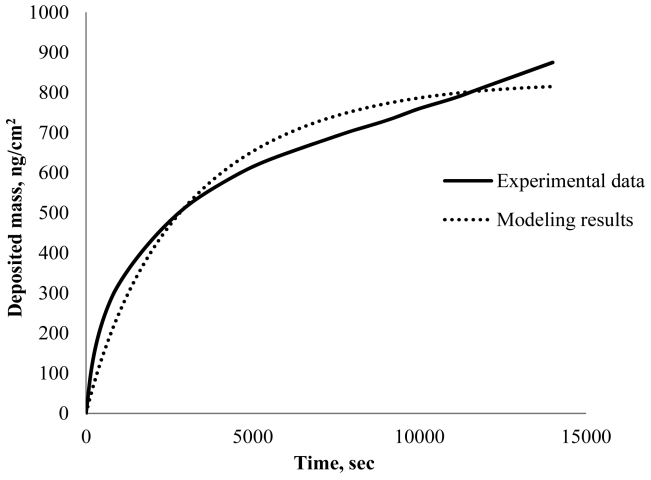

Figure 13. Experimental and modeling results of deposited mass from the 10 vol % crude oil + 90 vol % heptol solution with 90 vol % *n*-heptane onto a carbon steel surface at 20 °C and 80 μL/min flow rate.

From our previous paper (part 1; 10.1021/ef401857t), it is observed that the adsorption process is mostly controlled by the kinetics of adsorption at the initial time scale of the experiment. Thus, the slight offset between experimental and modeling results of deposited mass during the initial time in Figures 12 and 13 is because the dissolved asphaltene particles also play a role in the adsorption process. The experimental data are accordingly a little more than the model prediction, which considers only the precipitated asphaltene particles for deposition. After a long time (near 15 000 s), the model attains a saturated deposit amount, while the experimental data show that further deposition can occur (having not reached a saturation plateau). It should be recalled that the precipitation kinetics assumed in this work are simple first-order kinetics, which may not be sufficient to describe the precipitation of the polydisperse asphaltene. Different fractions of asphaltene may precipitate out at different rates, causing the presence of a deposit even after a long time.

The asphaltene concentration in the model oil is 100 ppm, while its concentration in the real oil systems is around 2.3 g/L (2300 ppm). However, the amount of deposited mass is in the same range as in Figures 4 and 5. It is to be noted that the depositing surfaces are not the same for the experimental data presented in Figures 4 and 5. Also, for the system with real oil, the solution is more bulky and viscous than the system with model oil. This results in reduced diffusion and deposition, which can be justified by comparing the parameters in Tables 3 and 4.

4.6. Deposition Model Sensitivity Analysis. To understand the effect of the diffusion coefficient and kinetic parameters on the shape and magnitude of the asphaltene deposit profile versus time, a sensitivity analysis is performed. The parameters used to model the amount of deposited mass versus time from a solution of 10 vol % crude oil + 90 vol % heptol with 80 vol % *n*-heptane are used as the base case, and each parameter is then varied individually to understand the effect of that particular parameter on the deposition profile. The effects of k_p, k_{ag}, k_d, and D on the asphaltene deposition profile are shown in Figures 14, 15, 16, and 17 respectively. The results are not clear in Figures 15 and 16 because of only a small change in deposited mass with changes in the aggregation and deposition kinetic constants. Hence, Figures 18 and 19 represent the changes in the deposited mass amount with higher changes of k_{ag} and k_d, respectively.

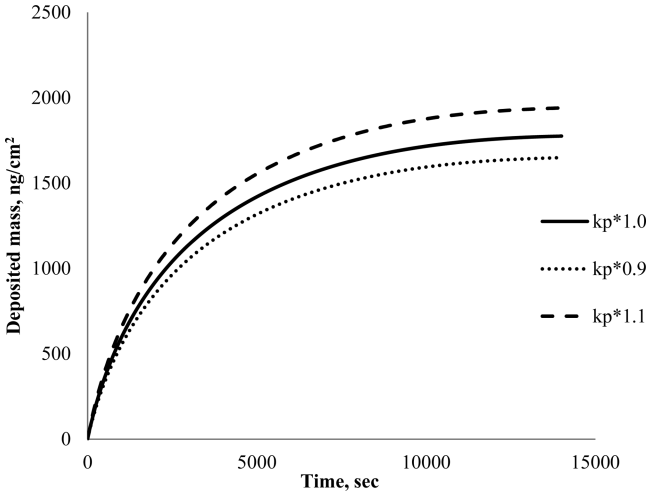

Figure 14. Effect of the precipitation kinetic constant, k_p, on the deposited mass amount versus time.

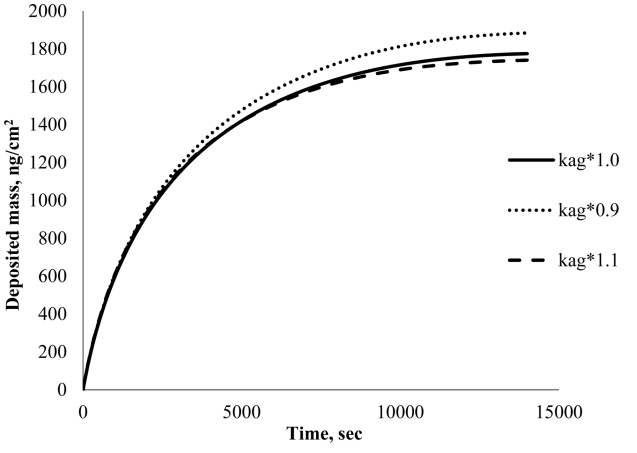

Figure 15. Effect of the aggregation kinetic constant, k_{ag}, on the deposited mass amount versus time.

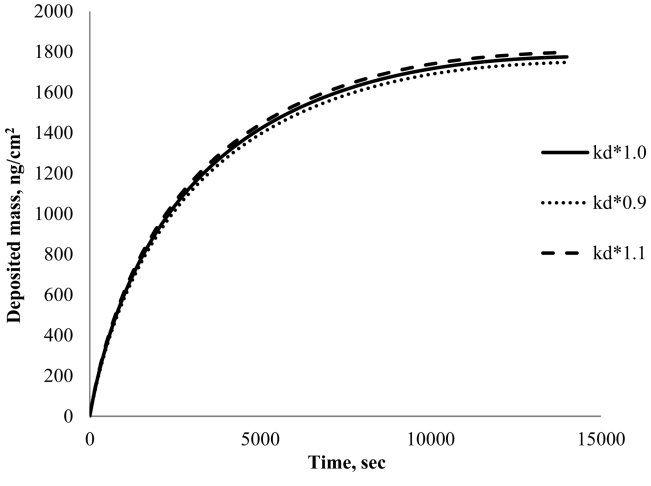

Figure 16. Effect of the deposition kinetic constant, k_d, on the deposited mass amount versus time.

It can be seen that the value of k_p has a very significant impact on the amount of deposited mass, as compared to those of k_{ag} and k_d. A small increase in k_p shows a significant increase in the amount of deposited mass versus time, and a decrease of k_p

dx.doi.org/10.1021/ef401868d | *Energy Fuels* 2014, 28, 3594−3603

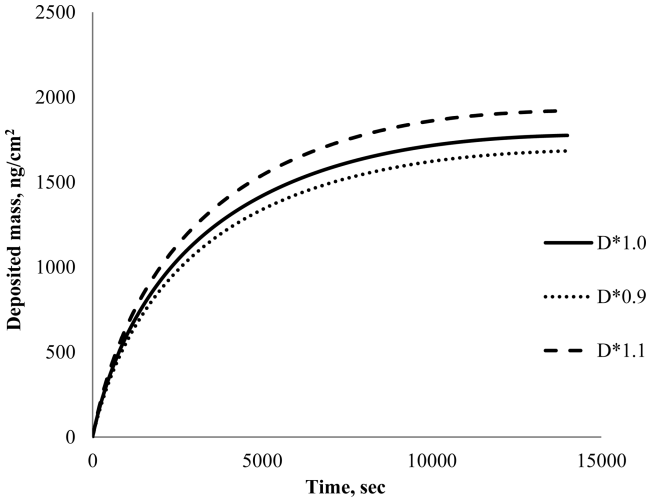

Figure 17. Effect of the diffusion coefficient, D, on the deposited mass amount versus time.

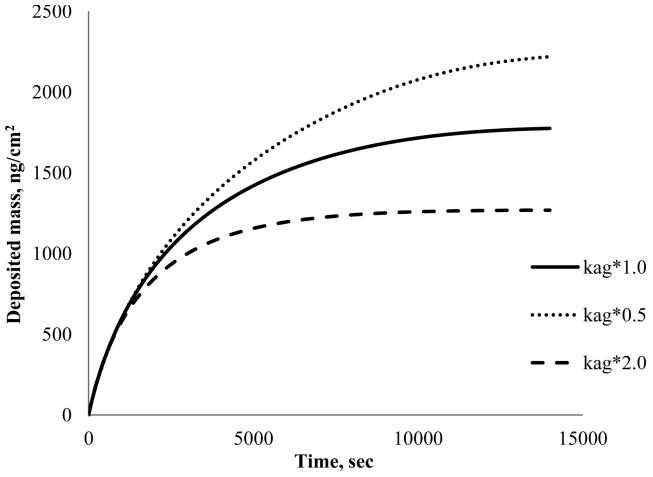

Figure 18. Effect on the deposited mass amount versus time with a large change in the aggregation kinetic constant, k_{ag}.

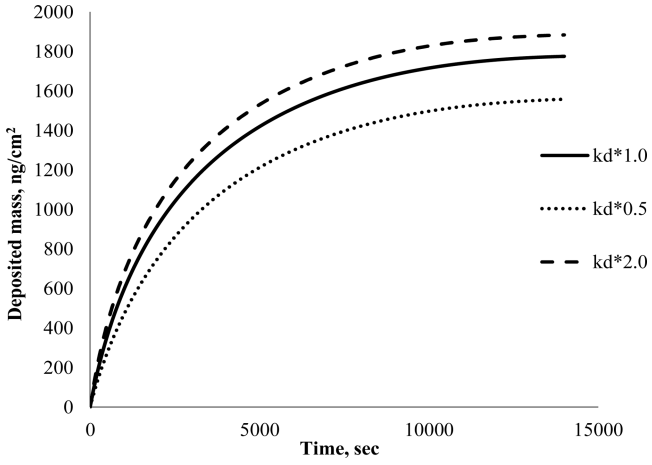

Figure 19. Effect on the deposited mass amount versus time with a large change in the kinetic constant of deposition, k_d.

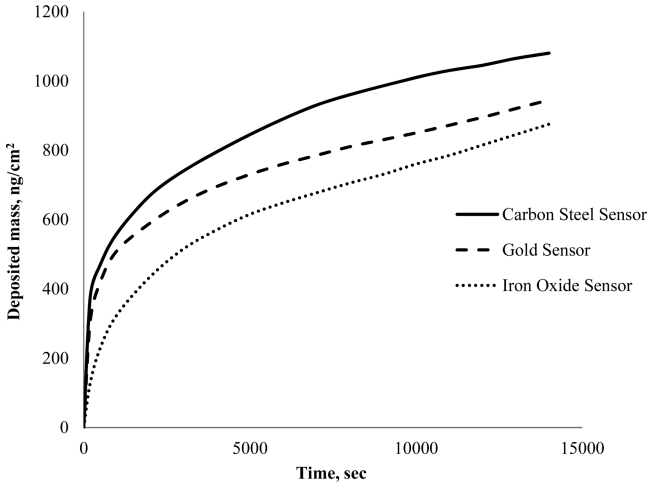

Figure 20. Amount of deposited mass from 10 vol % crude oil + 90 vol % *n*-heptane on different surfaces versus time at 20 °C and 80 μL/min flow rate.

results in a decrease of the deposited mass amount. Similar trends can be observed for the increase and decrease in the values of the diffusion coefficient, D, and deposition kinetic constant, k_d, as expected from the mechanism. A reverse trend is observed for the change in k_{ag}. When k_{ag} increases, the tendency of primary asphaltene particles to aggregate and form larger particles increases. Therefore, we have more numbers of larger particles, which can pass over the crystal surface without deposition because of convective transfer, and as a final result, we will have less amount of deposited mass versus time. It can be observed from Figure 18 that the effect of changes in k_{ag} on the deposited mass amount at the initial time scale is negligible, while the effects of changes in k_p and k_d are significant for all times.

4.7. Depositing Surface. To investigate the interaction between precipitated asphaltene from crude oil and pipeline material, carbon steel and iron oxide sensor crystals are used and compared to the gold surface. Many pipelines used for crude oil transport are made of carbon steel. Iron oxide presents the case of rust and can provide insight into the change in asphaltene deposition behavior because of a rusted pipeline compared to a new steel pipeline.

Figure 20 shows the amount of deposited mass from the 10 vol % crude oil + 90 vol % *n*-heptane system onto a gold, iron oxide, and carbon steel sensor crystal surface versus time at 20 °C and 80 μL/min flow rate. It can be interpreted from Figure 20 that both carbon steel and gold surfaces represent more deposited mass in comparison to the iron oxide surface. At the initial time, the amount of deposited mass onto a gold crystal is very close to the amount deposited onto a carbon steel surface. However, as time passes, the gold sensor shows less amount of deposited mass in comparison to the carbon steel surface. Furthermore, the amount of mass deposited on an iron oxide surface is less than that on a carbon steel sensor at all times.

For the carbon steel surface, the modeling result is already presented in Figure 13 using the adjustable parameters shown in Table 4. To model the experimental data of Figure 20, for the surfaces of gold and iron oxide, the same parameters used for the carbon steel case are used, except for k_d. This is because the operating conditions are the same for all of the cases, except for the depositing surface. To obtain a close match with experimental data, the values of k_d used corresponding to gold and iron oxide surfaces are 4.00×10^{-8} and 2.50×10^{-8} m/s. Both represent a lower value in comparison to the k_d used for the carbon steel sensor. Figures 21 and 22 show the experimental and modeling results for the amount of deposited mass versus time

dx.doi.org/10.1021/ef401868d | *Energy Fuels* 2014, 28, 3594−3603

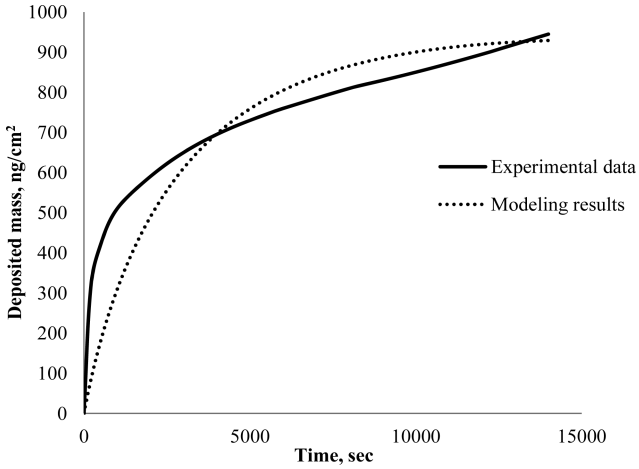

Figure 21. Experimental and modeling results for the amount of deposited mass versus time from a solution of 10 vol % crude oil + 90 vol % *n*-heptane onto a gold sensor at 20 °C and 80 μL/min flow rate.

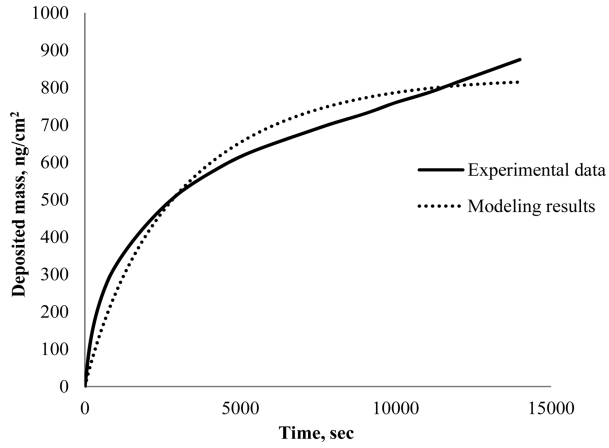

Figure 22. Experimental and modeling results for the amount of deposited mass versus time from a solution of 10 vol % crude oil + 90 vol % *n*-heptane onto an iron oxide sensor at 20 °C and 80 μL/min flow rate.

from a solution of 10 vol % crude oil + 90 vol % *n*-heptane onto gold and iron oxide surfaces, respectively.

In this work, the precipitation, aggregation, and deposition kinetic constants for the crude oil "S" are adjusted to reproduce the asphaltene deposition experimental data obtained using a QCM-D setup. Using these adjusted kinetic constants, one can use the previously developed asphaltene deposition tool (ADEPT) by Kurup et al. to measure the asphaltene deposition profile in wellbores and pipelines in a fully predictive manner.[11] However, first, a method needs to be developed for scaling the kinetic constant parameters from lab scale (QCM-D measurements) to field scale. Kurup et al. proposed a methodology for scaling up the deposition kinetic constant obtained from the capillary deposition experiments.[11] Scaling up the obtained kinetic constants from QCM-D experiments and linking between dynamic pipeline deposition and QCM-D deposition still need a good deal of work.

5. CONCLUSION

In this paper, QCM-D experiments are performed to study the depositional aspects of asphaltene from crude oil systems. The frequency and dissipation changes because of the deposited layer and after accounting for the liquid loading effect showed a viscoelastic behavior of the deposit. The following conclusions can be drawn from this study: (1) For the system of 10 vol % crude oil + 90 vol % heptol under consideration, the precipitation onset happens near 75 vol % heptane. (2) Modeling of experimental data before the asphaltene precipitation onset for the crude oil + heptol system showed that the adsorption process is controlled by adsorption kinetics in initial times. The adsorption process after a long time is governed by the diffusion and convective transfer. A rectangular adsorption isotherm is used, because all curves of deposited mass from crude oil reach equilibrium very soon. (3) When the ratio of heptane/toluene increases, the amount of asphaltene deposited mass from the corresponding heptol solution increases up to the precipitation onset and decreases beyond that. (4) After asphaltene precipitation, the transport of asphaltene over the crystal in the flow module may follow a multi-step process, including precipitation, aggregation, diffusion, advection, and deposition. To model the amount of deposited mass beyond the onset of asphaltene precipitation in a QCM-D experiment, a model is proposed with preliminary success for both model oil and real oil systems. (5) From the sensitivity analysis of kinetic parameters, the value of k_p has a very significant impact on the amount of deposited mass, as compared to those of k_{ag} and k_d. Increasing k_p increases the amount of deposited mass versus time and vice versa. A similar trend is observed for D and k_d, while an opposite trend is observed for the change in k_{ag} and consistent with the mechanism. (6) The effect of changes in k_{ag} on the deposited mass amount during the initial time scale is very small, while the effect of k_p and k_d is significant at all times. (7) In the presence of rust (iron oxide), the amount of deposited mass decreases with respect to a carbon steel surface. Both carbon steel and gold surfaces represent more deposited mass in comparison to the iron oxide surface. (8) For modeling of the experimental data with different surfaces but under the same operating conditions, the only parameter that needs to be adjusted between different cases is the kinetic constant of deposition, k_d.

The work presented in this paper can help to provide the deposition parameters for other asphaltene deposition simulators and, together with our previous paper (part 1; 10.1021/ef401857t), presents a complete experimental and modeling analysis of QCM-D asphaltene deposition.

AUTHOR INFORMATION

Corresponding Author

*Telephone: 001-713-348-4900. E-mail: wgchap@rice.edu.

Notes

The authors declare no competing financial interest.

ACKNOWLEDGMENTS

This work is undertaken with the funding from DeepStar and R&D Oil Subcommittee of Abu Dhabi National Oil Company. The authors are also thankful to Matthew Dixon, Mark Poggi, Jianxin Wang, Qilin Li, Lisa Biswal, Maura Puerto, Francisco Vargas, and Clarence Miller for experimental suggestions, lab space, access to equipment, and helpful discussions.

NOMENCLATURE

Δf = change in frequency
ΔD = change in energy dissipation
c = concentration of the asphaltene primary particle
x = coordinate in the direction of flow
y = coordinate in the direction normal to flow
t = time

V = axial linear velocity
$\langle V \rangle$ = average velocity
D = diffusion coefficient
c_i = concentration of asphaltene primary particles at initial conditions
c_0 = concentration of asphaltene in solution at the inlet
c^{eq} = concentration of dissolved asphaltene at equilibrium
k = rate constant
r = rate
f_0 = fundamental resonant frequency
n = overtone number
ρ = density
ν = shear wave velocity
μ = shear modulus
h = thickness
η = viscosity

Subscripts

x = coordinate in the direction of flow
y = coordinate in the direction normal to flow
p = precipitation
ag = aggregation
d = deposition
q = quartz
l = liquid
s = solvent

REFERENCES

(1) Tavakkoli, M.; Panuganti, S. R.; Vargas, F. M.; Taghikhani, V.; Pishvaie, M. R.; Chapman, W. G. *Energy Fuels* **2014**, *28*, 1617−1628.
(2) Abudu, A.; Goual, L. *Energy Fuels* **2009**, *23*, 1237−1248.
(3) Jaramillo, E.; Galeana, C. L.; Manero, O. *Energy Fuels* **2006**, *20*, 1184−1196.
(4) Akbarzadeh, K.; Ratulowski, J.; Lindvig, T.; Davies, T.; Huo, Z.; Broze, G. *Proceedings of the SPE Annual Technical Conference and Exhibition*; New Orleans, LA, Oct 4−7, 2009; SPE 124956.
(5) Jamialahmadi, M.; Soltani, B.; Steinhagen, H. M.; Rashtchian, D. *Int. J. Heat Mass Transfer* **2009**, *52*, 4624−4634.
(6) Zhu, H.; Jing, J.; Che, J.; Li, Q.; Yu, X. *Proceedings of the IEEE International Conference*; Chengdu, China, July 9−11, 2010.
(7) Sileri, D.; Sahu, K.; Ding, H.; Matar, O. K. *Proceedings of the International Conference on Heat Exchanger Fouling and Cleaning*; Schladming, Austria, June 14−19, 2009.
(8) Eskin, D.; Ratulowski, J.; Akbarzadeh, K.; Pan, S.; Lindvig, T. *Proceedings of the International Conference on Multiphase Flow*; Tampa, FL, May 30−June 4, 2010.
(9) Vargas, F. M.; Creek, J. L.; Chapman, W. G. *Energy Fuels* **2010**, *24*, 2294−2299.
(10) Kurup, A. S.; Vargas, F. M.; Wang, J.; Buckley, J. S.; Creek, J. L.; Subramani, H. J.; Chapman, W. G. *Energy Fuels* **2011**, *25*, 4506−4516.
(11) Kurup, A. S.; Wang, J.; Subramani, H. J.; Buckley, J. S.; Creek, J. L.; Chapman, W. G. *Energy Fuels* **2012**, *26*, 5702−5710.
(12) Andersson, F. *Q-Sense Webinar*, Dec 10, 2012.
(13) Filippov, L. K. *J. Colloid Interface Sci.* **1995**, *174*, 32−39.
(14) Panuganti, S. R.; Vargas, F. M.; Gonzalez, D. L.; Kurup, A. S.; Chapman, W. G. *Fuel* **2012**, *93*, 658−669.
(15) Punnapala, S.; Vargas, F. M. *Fuel* **2013**, *108*, 417−429.
(16) Panuganti, S. R.; Vargas, F. M.; Chapman, W. G. *Energy Fuels* **2012**, *26*, 2548−2557.
(17) Panuganti, S. R.; Tavakkoli, M.; Vargas, F. M.; Gonzalez, D. L.; Chapman, W. G. *Fluid Phase Equilib.* **2013**, *359*, 2−16.
(18) Kanazawa, K. K.; Gordon, J. G., II. *Anal. Chem.* **1985**, *57*, 1770−1771.
(19) Tavakkoli, M.; Panuganti, S. R.; Taghikhani, V.; Pishvaie, M. R.; Chapman, W. G. *Fuel* **2014**, *117*, 206−217.
(20) Rajagopal, K.; Silva, S. M. C. *Braz. J. Chem. Eng.* **2004**, *21*, 601−609.